KERNEL REGRESSION FOR HEAD-RELATED TRANSFER FUNCTION INTERPOLATION AND SPECTRAL EXTREMA EXTRACTION

Yuancheng Luo, Dmitry N. Zotkin, Hal Daumé III, Ramani Duraiswami

Department of Computer Science
University of Maryland, College Park
College Park, MD 20742 USA

ABSTRACT

Head-Related Transfer Function (HRTF) representation and interpolation is an important problem in spatial audio. We present a kernel regression method based on Gaussian process (GP) modeling of the joint *spatial-frequency* relationship between HRTF measurements and obtain a smooth non-linear representation based on data measured over both arbitrary and structured spherical measurement grids. This representation is further extended to the problem of extracting spectral extrema (notches and peaks). We perform HRTF interpolation and spectral extrema extraction using freely available CIPIC HRTF data. Experimental results are shown.

Index Terms— Gaussian Process Regression, Head-Related Transfer Function, Interpolation, Spectral Extrema.

1. INTRODUCTION

The human ability to accurately localize a three-dimensional sound source is due to the fact that the source's acoustic wave scatters on the listener's anatomic features (torso, head, and outer ears). Because of asymmetries of those features, the scattering pattern – and thus the sound that actually reaches the eardrum – depends on the direction of sound arrival. The quantitative measure of how the sound is modified by such scattering is called Head-Related Transfer Function (HRTF) [1]. HRTF knowledge enables one to reconstruct life-like auditory scenes; however, due to physical differences between individuals, HRTF is largely person-specific.

Many research labs around the world have measured HRTF for actual human subjects. The common feature of those measurements is that they have very little in common. Indeed, each lab has its own measurement apparatus; its own sampling frequency, excitation signal, and operating environment; and most importantly its own HRTF measurement grid. The latter is particularly troublesome because high-quality spatial audio reproduction of a moving acoustic source requires an HRTF measured at uniformly high spatial resolution, which is rarely the case due to time/cost issues and peculiarities of each particular measurement setup/process (in particular, the area below the subject, referred to later as the *bottom hole*, is almost never measured except for some mannequin studies; Figure 1 illustrates a typical HRTF measurement grid).

We propose a non-parametric, joint spatial-frequency HRTF representation that is well-suited for interpolation and can be easily manipulated. The model uses prior data (i.e., HRTF measurements) to infer HRTF for a previously unseen location or frequency. While this approach is general enough to consider the HRTF personalization problem, here we apply it to representing a single-subject HRTF. In section 2, we formulate the interpolation problem as a Gaussian process regression (GPR) [2] between the input spatial-frequency coordinate domain (ω, θ, ϕ) and the output HRTF measurement[1] $H_\omega(\theta, \phi)$.

The GPR approach is non-parametric but does require the specification of a covariance model, which should reflect prior knowledge about the problem. Empirical observations suggest that HRTF generally varies smoothly both over space and over frequency coordinates. In section 3, two covariance functions are presented to model HRTF smoothness. GPR also enjoys the advantage of automatic model selection via marginal-likelihood optimization using Bayesian inference – a feature that other methods do not possess. Our model also has a natural extension to the automatic extraction of spectral extrema (such as peaks and notches) used in [5, 6] for simplifying the HRTF representation. In section 4, we outline the extrema localization algorithm. Finally, in section 5 we compare our model to other spherical interpolation techniques [7, 8] using the CIPIC database [9] data and illustrate the behavior of the extrema extraction algorithm for varying values of noise estimate in GPR.

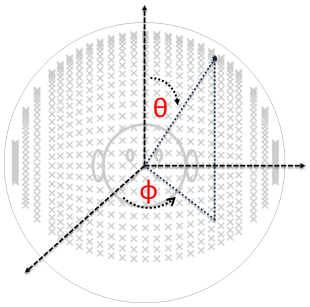

Fig. 1. Sample (CIPIC database) HRTF measurement grid.

Related Work: The simplest HRTF interpolation methods operate in frequency domain and perform weighted averaging of nearby HRTF measurements [10, 11, 12] using the great-circle distance; smoothness constraint is not addressed. More advanced methods are based on spherical splines [13, 14]; these methods attempt to fit the data points while keeping the resulting interpolation surface smooth. Other interpolation methods represent HRTF as a series of spherical harmonics [15, 16] (which has the advantage of obtain-

Support of NSF award IIS-1117716 is gratefully acknowledged.

Dr. Zotkin is with Institute for Advanced Computer Studies (UMIACS), University of Maryland, College Park.

[1] Through the current paper, we use the term *HRTF measurement* to refer exclusively to the magnitude part as HRTF can be reconstructed from magnitude response using min-phase transform and pure time delay [3, 4].

ing physically-correct interpolation but is hard to apply in the typical case of bottom-hole measurement grid) or decompose HRTF in the principal component space [17, 18] and interpolate the decomposition coefficients over nearby spatial positions. In all of these methods, smoothness over frequency coordinate is not considered. The recent paper [19] has introduced a method of further decomposing the spherical harmonics representation into a series on frequency axis as well, implicitly making the interpolant smooth as the consequence of smoothness of the spectral basis functions. In the GPR method proposed in the current paper, we make the combined spatio-spectral smoothness constraint explicit, derive the corresponding theory, and compare our approach with the ones above in terms of interpolation/approximation error.

2. GAUSSIAN PROCESS REGRESSION

In a general regression problem, one predicts a scalar target variable y from a D-dimensional vector x of independent variables based on a collection of available observations (measurements). A common model assumes that the observation y is generated by an unknown latent function $f(x)$ and is corrupted by additive (Gaussian) noise

$$y = f(x) + \epsilon, \quad \epsilon \sim \mathcal{N}(0, \sigma^2), \tag{1}$$

where the noise term ϵ is zero centered with constant variance σ^2. Placing a GP prior distribution on the latent function $f(x)$ enables inference and encodes several useful properties such as local smoothness, stationarity, and periodicity. For any subset of inputs $X = [x_1, \ldots, x_N]$, the corresponding vector of function values $\mathbf{f} = [f(x_1), f(x_2), \ldots, f(x_N)]$ has a joint N-dimensional Gaussian distribution that is specified by the prior mean $m(x)$ and covariance $K(x_i, x_j)$ functions

$$\begin{aligned} f(x) \sim GP(m(x), K(x_i, x_j)), \quad m(x) = 0, \\ K(x_i, x_j) = \text{Cov}(f(x_i), f(x_j)). \end{aligned} \tag{2}$$

The joint distribution between N training outputs y and N_* test outputs f_* under the GP prior is

$$\begin{aligned} \begin{bmatrix} y \\ f_* \end{bmatrix} \sim \mathcal{N}\left(0, \begin{bmatrix} K(X,X) + \sigma^2 I & K(X, X_*) \\ K(X_*, X) & K(X_*, X_*) \end{bmatrix}\right), \\ K_{ff} = K(X,X), \quad \hat{K} = K_{ff} + \sigma^2 I, \\ K_{f*} = K(X, X_*), \quad K_{**} = K(X_*, X_*), \end{aligned} \tag{3}$$

where $K(X,X)$ and $K(X,X_*)$ are $N \times N$ and $N \times N_*$ matrices of covariances evaluated at all pairs of training and test inputs respectively. From Eq. 3 and marginalization over the function space $\mathbf{f}$, it is known that the set of test outputs conditioned on the test inputs, training data, and training inputs is a normal distribution given by

$$\begin{aligned} P(f_*|X, y, X_*) \sim \mathcal{N}(\bar{f}_*, \text{cov}(f_*)), \\ \bar{f}_* = E[f_*|X, y, X_*] = K_{f*}^T \hat{K}^{-1} y, \\ \text{cov}(f_*) = K_{**} - K_{f*}^T \hat{K}^{-1} K_{f*}. \end{aligned} \tag{4}$$

Thus, the interpolant $\bar{f}_*$ for inputs X_* in Eq. 4 is computed from the inversion of the covariance matrix $\hat{K}$ specified by the covariance function K, its hyperparameters, and control points (i.e. training outputs y). Model-selection is an O(N^3) runtime task of minimizing the gradient of the negative log-marginal likelihood function w.r.t. a hyperparameter Θ_i:

$$\begin{aligned} \log p(y|X) = -\frac{1}{2}\left(\log|\hat{K}| + y^T \hat{K}^{-1} y + N \log(2\pi)\right), \\ \frac{\partial \log p(y|X)}{\partial \Theta_i} = -\frac{1}{2}\left(\text{tr}\left(\hat{K}^{-1} P\right) - y^T \hat{K}^{-1} P \hat{K}^{-1} y\right), \end{aligned} \tag{5}$$

where $P = \partial \hat{K} / \partial \Theta_i$ is the matrix of partial derivatives.

3. COVARIANCE FUNCTIONS

The GP prior covariance function encodes the assumed constraints on the latent function f. In particular, the degree of correlation between any subset of outputs (i.e., the smoothness, which is the desired interpolation property) is fully specified by the GP prior as a function over the input domain and a hyperparameter set. We propose to model the single magnitude HRTF as an *Ornstein-Uhlenbeck* (OU) [20] process, resulting in a GP with stationary auto-covariance and spectral density functions

$$K_t(t_i, t_j) = e^{-|t_i - t_j|/\lambda}, \quad K_\omega(\omega_i, \omega_j) = \frac{1}{\lambda^2 + (\omega_i - \omega_j)^2}, \tag{6}$$

where (t, ω) are time and frequency (inputs) and λ the *characteristic length-scale* hyperparameter. The λ term in the OU process is the rate of mean reversion or drift to zero of a solution to a stochastic differential equation with standard Brownian motion. OU description agrees with the fact that the HRTF in time domain decays quickly to zero after the initial onset and is thus reasonable.

For estimating the joint magnitude responses for the same frequency, the spatial component of the cross-spectral density can be modeled as a function of spherical coordinates (θ, ϕ) that must be expressible in the proper spherical basis [21]. The family of isotropic covariances restricted to distances in $\mathbb{R}^3$ as chordal C_h given by

$$C_h = 2\sqrt{\sin^2\left(\frac{\theta_j - \theta_i}{2}\right) + \sin\theta_i \sin\theta_j \sin^2\left(\frac{\phi_i - \phi_j}{2}\right)}, \tag{7}$$

is valid on the unit sphere [22, 23]. The hyperparameter ℓ can be interpreted as the distance for function values to become uncorrelated w.r.t. an axis in the input domain. We remark that the covariance function's relation to the spherical harmonics basis $Y_n^m(\theta, \phi)$ follows the Legendre addition theorem,

$$K(\theta_i, \theta_j, \phi_i, \phi_j) = \sum_{n=0}^{\infty} b_n \frac{4\pi}{2n+1} \sum_{m=-n}^{n} Y_n^m(\theta_i, \phi_i) \bar{Y}_n^m(\theta_j, \phi_j),$$

where coefficient b_n depends on the choice and parameterization of K. This provides a way to represent the GP interpolant $\bar{f}_*$ in the spherical harmonics basis (as it is just a weighted combination of covariance evaluations).

3.1. Frequency-Independent Model

First, we consider the case of frequency independent GP. For a frequency ω, the function $\mathbf{f}_\omega$ with a GP stationary isotropic exponential covariance prior $K_\omega(\theta_i, \theta_j, \phi_i, \phi_j) = \alpha_\omega^2 e^{-C_h/\ell_\omega^2}$ is independently specified over a set of spatial locations T_N. The hyperparameters $(\ell_\omega, \alpha_\omega)$ are trained independently at each frequency via log-marginal likelihood optimization of the HRTF measurements following Eq. 5, and prediction of posterior means at new spatial-frequency locations $X_* = (\theta_*, \phi_*, w_*)$ requires the evaluation of $\bar{f}_{\omega *}$ in Eq. 4 using the available measurements on T_N.

Figure 2 presents sample CIPIC database HRTF plots for a single frequency using a Mercator projection from the sphere to a cylinder. The GP length-scale hyperparameters are trained in 50 iterations and the noise estimate $\sigma = 0.05$ is fixed. Note that the input data set contains no measurements below a certain elevation and that the sampling is denser near the interaural poles. The posterior means

(i.e., the interpolated HRTF) over the full sphere of directions, including the bottom hole, are generated by inference (top plot). The posterior variances (bottom plot) depend only on the measurement point spacing. It can be seen that a contour map outlines an area of high confidence (dense areas around the poles) and another, low confidence one (bottom hole where measurements are absent).

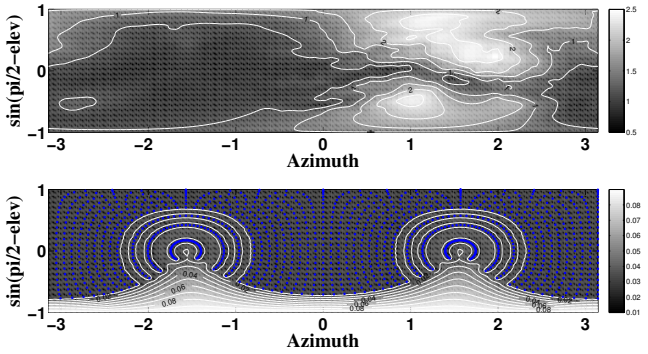

Fig. 2. GP mean (top) and variance (bottom) at 7.5 kHz. Data: CIPIC subject 003, right ear. Blue markers are the control points.

3.2. Joint Spatial-Frequency Model

In the more complicated case of a joint spatial-frequency covariance function, we specify the single GP covariance prior for the function $\mathbf{f}$ as the product of OU density in Eq. 6 and exponential covariance function of chordal distance in Eq. 7 given by

$$K(\theta_i, \theta_j, \phi_i - \phi_j, \omega_i - \omega_j) = \frac{\alpha^2}{\lambda^2 + (\omega_i - \omega_j)^2} e^{-C_{h_{ij}}/\ell^2}, \quad (8)$$

To reduce computational complexity, we decompose the matrix K_{ff} into Kronecker tensor products $K_{ff} = K_1 \otimes K_2$, where matrices K_1 and K_2 are covariance evaluations in the spatial and frequency domain respectively. The inverse covariance matrix with additive white noise is given by the Kronecker product eigendecomposition

$$\begin{aligned} \hat{K}^{-1} &= (UZU^T + \sigma^2 I)^{-1} = U(Z + \sigma^2 I)^{-1} U^T, \\ K_i &= U_i Z_i U_i^T, \quad U = U_1 \otimes U_2, \quad Z = Z_1 \otimes Z_2, \end{aligned} \quad (9)$$

which consist of eigendecompositions of smaller covariance matrices $K_i \in \mathbb{R}^{m_i \times m_i}$; the total number of samples is $N = \prod_{i=1}^{2} m_i$. Efficient Kronecker methods [24] reduce costs of inference and hyperparameter training in Eqs. 4 and 5 from $O(N^3)$ to $O(\sum_{i=1}^{2} m_i^3 + N \sum_{i=1}^{2} m_i)$ and storage from $O(N^2)$ to $O(N + \sum_{i=1}^{2} m_i^2)$.

This formulation allows the whole HRTF set of a single subject to be jointly modeled as a Gaussian distribution in a tractable manner under the assumption that the hyperparameters (α, λ, ℓ) do not vary over space and frequency. The shared noise parameter σ can be estimated as well by treating it as a hyperparameter in Eq. 5. Inference at a new input $X_* = (\omega_*, \theta_*, \phi_*)$ is the direct evaluation of $\bar{f}_*$ in Eq. 4.

4. SPECTRAL EXTREMA EXTRACTION

By definition, the spectral extrema correspond to the zero-crossing of the GP interpolant gradient. The surface gradient and the necessary covariance derivatives w.r.t. frequency ω_* are expressed in the closed form as

$$\begin{aligned} \frac{\partial \bar{f}_*}{\partial \omega_*} &= \left[\frac{\partial K_{1*}}{\partial \omega_*}, \ldots, \frac{\partial K_{N*}}{\partial \omega_*} \right] \hat{K}^{-1} y, \\ \frac{\partial K_{i*}}{\partial \omega_*} &= \frac{-2\alpha^2(\omega_* - \omega_i)}{(\lambda^2 + (\omega_* - \omega_i)^2)^2} e^{-C_{h\,i*}/\ell^2}, \\ \frac{\partial^2 K_{i*}}{\partial \omega_*^2} &= \frac{-2\alpha^2(\lambda^2 - 3(\omega_* - \omega_i)^2)}{(\lambda^2 + (\omega_* - \omega_i)^2)^3} e^{-C_{h_{i*}}/\ell^2}. \end{aligned} \quad (10)$$

Zero-crossings of the gradient signify spectral notches and peaks; these can be further distinguished by the sign of the second derivative. The second partial derivative can be computed in a similar fashion. We use an iterative *Newton-Raphson* method

$$\omega_{n+1} = \omega_n - \frac{\partial \bar{f}_{\omega_n}}{\partial \omega_n} / \frac{\partial^2 \bar{f}_{\omega_n}}{\partial \omega_n^2}, \quad |\omega_{n+1} - \omega_n| > \tau, \quad (11)$$

for locating zeros of the interpolant gradient in Eq. 10. The method was found to converge in a few iterations using a termination threshold of 10^{-5}. The initial guesses ω_0 are spaced uniformly in the frequency domain.

5. EXPERIMENTS

We use data from the CIPIC database (subject 003, right ear) in the experimental evaluation; HRTF is computed using DFT of the 200-sample impulse response. The measure of the interpolation error is the signal-to-distortion ratio (SDR) [25] at test directions given by

$$\text{SDR}_\omega = 10 \log_{10} \frac{\sum_{i=1}^{N_*} H_\omega(\theta_i, \phi_i)^2}{\sum_{i=1}^{N_*} (H_\omega(\theta_i, \phi_i) - \hat{H}_\omega(\theta_i, \phi_i))^2}, \quad (12)$$

where $H_\omega(\theta_i, \phi_i) = y_{\omega, \theta_i, \phi_i}$ is the observation and $\hat{H}_\omega(\theta_i, \phi_i) = \bar{f}_{\omega, \theta_i, \phi_i}$ in Eq. 4 the predicted magnitude responses at frequency ω in direction (θ_i, ϕ_i). GP hyperparameters are trained using gradient descent with resilient back-propagation [26] for 50 iterations. The accuracy of GPR interpolation is evaluated in comparison with that of weighted nearest-neighbor, spherical spline, and spherical harmonics based interpolation methods.

5.1. HRTF Interpolation

In the first experiment, randomly-chosen half of 1250 CIPIC grid directions comprise the "measurement" data set for each subject; covariance hyperparameters are trained and GPR infers the remaining directions and returns the prediction error. The task measures how well the global interpolant is suited for the case of a randomized measurement grid. SDR plots for each interpolation methods are shown in Figure 3; high SDR corresponds to a good reconstruction. For the spherical spline method [27], the default parameters for smoothing ($\lambda = 1e-5$) and expansion terms (50) are used. For the spherical harmonic fitting [15], truncated SVD regularization method is used as described. The results show that both frequency-independent and joint spatial-frequency GPR models with Bayesian model selection outperforms all other methods in the $2 - 20$ kHz frequency range.

For the second experiment, we simulate missing data in a large spatial area (an open hole task [28]). We remove all measurements that lie above certain horizontal plane (spherical incident angle $\theta < \pi/5$), essentially cutting off the top portion of the sphere of direction. There are a total of 147 measurement directions in the cut-off area.

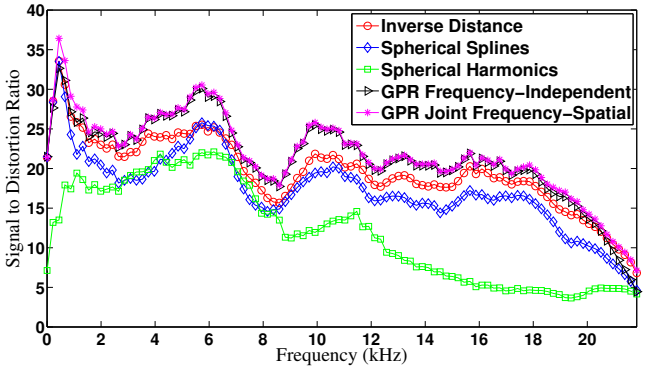

Fig. 3. SDR (dB) for the random half-set interpolation task. Larger values indicate better performance.

The interpolant is computed over the rest of measurements, is evaluated in the hole area, and the SDR is computed. This task simulates the HRTF prediction in the areas where data is not available (such as the bottom hole in most HRTF measurement grids). The SDR across each frequency are shown in Figure 4. Our two GPR models exhibit similar performance and are better than other methods across most of the frequency range. The loss of accuracy in the $12-16$ kHz band for global interpolation methods is due to the fact that at those frequencies, the head shape related HRTF features in "above-head" area become almost independent of pinna-related features prominent at low elevations. Non-stationary and non-separable cross frequency-spatial covariances may be necessary to further improve (decrease predicted variance along missing directions) our joint model over the frequency-independent approaches.

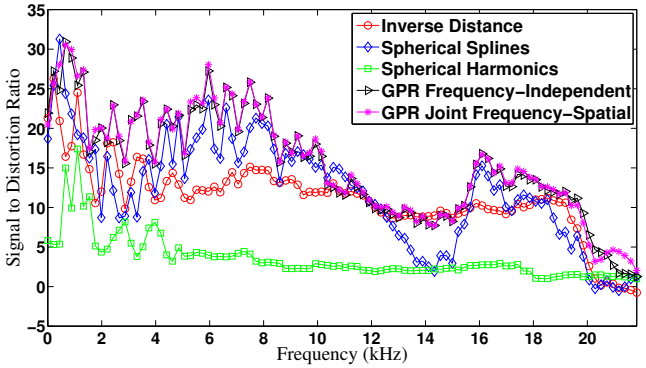

Fig. 4. SDR (dB) for the hole extrapolation task.

5.2. Extraction of Spectral Features

The spectral extrema extraction process in section 4 depends on the GP interpolant and its trained hyperparameters. The noise estimate σ could be learned within the GP model; however, often it is simply set to a fixed value using prior knowledge, enforcing a certain degree of smoothness on the interpolant. An example of how varying the noise term influences the interpolant and its extrema is shown in Figure 5. When the noise term σ is small, the GP predicted means tend towards observations. As it increases, the interpolant is allowed greater deviation and the number of extrema found becomes smaller;

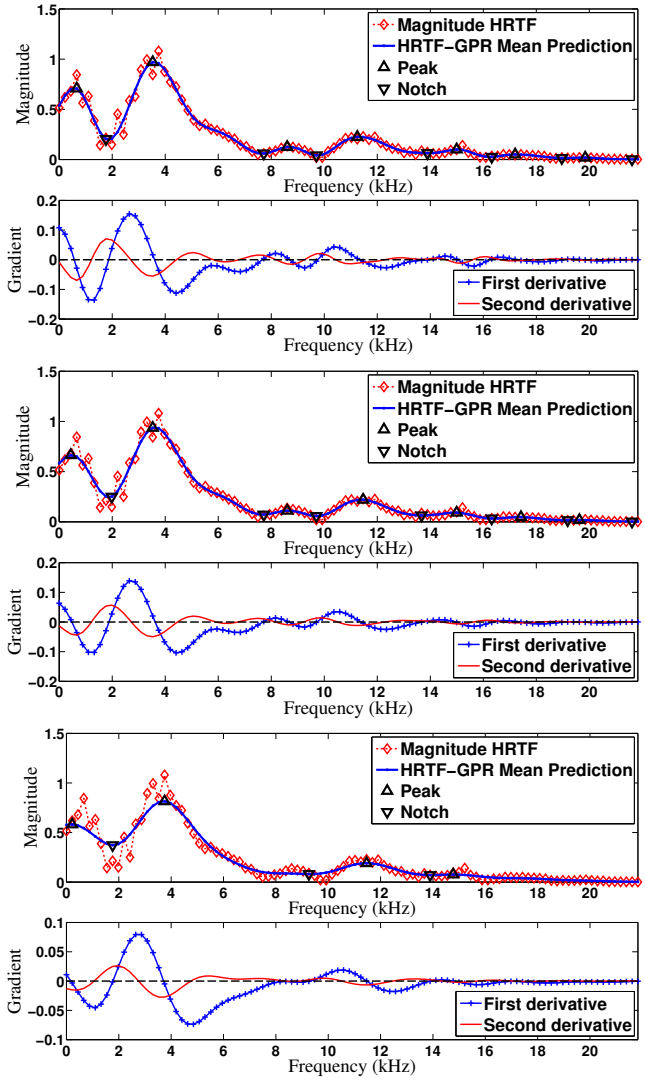

Fig. 5. GP spectral extrema extraction example. Data: CIPIC subject 003, right ear, direction $(87.6°, -65.1°)$. Top 2 plots: $\sigma = 0.05$. Middle 2 plots: $\sigma = 0.10$. Bottom two plots: $\sigma = 0.20$.

only the most salient peaks and notches are detected with large σ because of the smoothing effect. The phenomenon is apparent for many extrema in the $8-20$ kHz that are present in $\sigma = \{0.05, 0.1\}$ case but disappear for $\sigma = 0.2$. Thus, the consistency of extrema at various values of σ can be interpreted as a measure of salience along the corresponding frequencies.

6. CONCLUSIONS

We have presented a joint spatial-frequency GPR model with separable covariances for a single-subject HRTF representation and interpolation. The proposed method achieves better interpolation/extrapolation accuracy in comparison with other existing spherical interpolation methods. We extended the GPR model to HRTF spectral extrema extraction and explored a saliency metric using different GPR noise estimates. Future work is planned for more complex joint covariance models and multi-subject personalization.

7. REFERENCES

[1] D. N. Zotkin, R. Duraiswami, and L. S. Davis, "Rendering localized spatial audio in a virtual auditory space," *IEEE Transactions on Multimedia*, vol. 6, pp. 553–564, 2004.

[2] C. E. Rasmussen and C. Williams, *Gaussian Processes for Machine Learning*, MIT Press, Cambridge, Massachusettes, 2006.

[3] D. J. Kistler and F. L. Wightman, "A model of head-related transfer functions based on principal components analysis and minimum-phase reconstruction," *Journal of Acoustical Society of America*, vol. 91, pp. 1637–1647, 1992.

[4] A. Kulkarni, S. K. Isabelle, and H. S. Colburn, "Sensitivity of human subjects to head-related transfer-function phase spectra," *Journal of the Acoustical Society of America*, vol. 105, pp. 2821–2840, 1999.

[5] V. C. Raykar, R. Duraiswami, and B. Yegnanarayana, "Extracting the frequencies of the pinna spectral notches in measured head related impulse responses," *Journal of Acoustical Society of America*, vol. 118, pp. 364–374, 2005.

[6] V. R. Algazi, C. Avendano, and R. O. Duda, "Elevation localization and head-related transfer function analysis at low frequencies," *Journal of the Acoustical Society of America*, vol. 109, pp. 1110–1122, 2001.

[7] R. Duraiswami, D. N. Zotkin, and N. A. Gumerov, "Interpolation and range extrapolation of HRTFs," in *IEEE ICASSP*, Montreal, QC, Canada, 2004, vol. 4, pp. 45–48.

[8] S. M. Robeson, "Spherical methods for spatial interpolation: Review and evaluation," *Cartography and Geographic Information Science*, vol. 24, pp. 3–20, 1997.

[9] V. R. Algazi, R. O. Duda, and C. Avendano, "The CIPIC HRTF Database," in *IEEE Workshop on Applications of Signal Processing to Audio and Acoustics*, New Paltz, NY, 2001, pp. 99–102.

[10] L. Savioja, J. Huopaniemi, T. Lokki, and R. Väänänen, "Creating interactive virtual acoustic environments," *Journal of the Audio Engineering Society*, vol. 47, pp. 675–705, 1999.

[11] D. R. Begault, "3D sound for virtual reality and multimedia," *Academic Press, Cambridge, MA*, 1994.

[12] F. P. Freeland, L. Wagner, P. Biscainho, and P. R. Dinz, "Efficient HRTF interpolation in 3D moving sound," 2002, pp. 106–114.

[13] F. Perrin, J. Pernier, O. Bertrand, and J. F. Echallier, "Spherical splines for scalp potential and current density mapping," *Electroencephalogr Clin Neurophysiol*, vol. 72, pp. 184–7, 1989.

[14] G. Wahba, "Spline interpolation and smoothing on the sphere," *SIAM Journal on Scientific Statistical Computing*, vol. 2, pp. 5–16, 1981.

[15] D. N. Zotkin, R. Duraiswami, and N. A. Gumerov, "Regularized HRTF fitting using spherical harmonics," in *IEEE Workshop on Applications of Signal Processing to Audio and Acoustics*, 2009, pp. 257–260.

[16] W. Zhang, M. Zhang, R. A. Kennedy, and T. D. Abhayapala, "On high-resolution head-related transfer function measurements: An efficient sampling scheme," *IEEE Transcations on Audio, Speech, and Language Processing*, vol. 20, pp. 575–584, 2012.

[17] L. Wang, F. Yin, and Z. Chen, "Head-related transfer function interpolation through multivariate polynomial fitting of principal component weights," *Acoustical Science and Technology*, vol. 30, pp. 395–403, 2009.

[18] J. Cheng, B. D. Van Veen, and K. E. Hecox, "A spatial feature extraction and regularization model for the head related transfer function," *Journal of Acoustical Society of America*, vol. 97, pp. 439–452, 1995.

[19] W. Zhang, R. A. Kennedy, and T. D. Abhayapala, "Efficient continuous HRTF model using data independent basis functions: Experimentally guided approach," *IEEE Transcations on Audio, Speech, and Language Processing*, vol. 17, pp. 819–829, 2009.

[20] G. E. Uhlenbeck and L. S. Ornstein, "On the theory of Brownian motion," *Phys. Rev*, vol. 36, pp. 823–841, 1930.

[21] C. Huang, H. Zhang, and S. M. Robeson, "On the validity of commonly used covariance and variogram functions on the sphere," *Mathematical Geosciences*, vol. 43, pp. 721–733, 2011.

[22] A. M. Yaglom, "Correlation theory of stationary and related random functions vol. I: Basic results," *Springer Series in Statistics. Springer-Verlag*, 1987.

[23] T. Gneiting, "Correlation functions for atmospheric data analysis," *Quarterly Journal of the Royal Meteo-rological Society*, vol. 125, pp. 2449–2464, 1999.

[24] Y. Saatci, *Scalable Inference for Structured Gaussian Process Models*, Ph.D. thesis, University of Cambridge, 2011.

[25] F. Keyrouz and K. Diepold, "A rational HRTF interpolation approach for fast synthesis of moving sound," in *12th Digital Signal Processing Workshop and 4th Signal Processing Education Workshop*, 2006, pp. 222–226.

[26] M. Riedmiller, "RPROP: Description and implementation details," Tech. Rep., University of Karlsruhe, 1994.

[27] J. Kayser and C. E. Tenke, "Principal components analysis of Laplacian waveforms as a generic method for identifying ERP generator patterns: I. Evaluation with auditory oddball tasks.," *Clinical Neurophysiology*, vol. 117, pp. 348–368, 2006.

[28] W. Zhang, R. A. Kennedy, and T. D. Abhayapala, "Iterative extrapolation algorithm for data reconstruction over sphere," in *IEEE International Conference on Acoustics, Speech, and Signal Processing (ICASSP)*, 2008, pp. 3733–3736.